frontiers | Frontiers in Sustainable Food Systems

ORIGINAL RESEARCH
published: 04 July 2022
doi: 10.3389/fsufs.2022.934552

Decay of Trichomes of *Arthrospira platensis* After Permeabilization Through Pulsed Electric Fields (PEFs) Causes the Release of Phycocyanin

Justus Knappert[1]*, *Jonas Nolte*[1], *Natalya Friese*[1], *Ye Yang*[1], *Christoph Lindenberger*[2], *Cornelia Rauh*[1] and *Christopher McHardy*[1]

[1] Department of Food Biotechnology and Food Process Engineering, Technische Universität Berlin, Berlin, Germany, [2] Department of Mechanical Engineering/Environmental Technology, Ostbayerische Technische Hochschule (OTH) Amberg-Weiden, Amberg, Germany

The cyanobacterium *Arthrospira platensis* is a promising source of edible proteins and other highly valuable substances such as the blue pigment-protein complex phycocyanin. Pulsed electric field (PEF) technology has recently been studied as a way of permeabilizing the cell membrane, thereby enhancing the mass transfer of water-soluble cell metabolites. Unfortunately, the question of the release mechanism is not sufficiently clarified in published literature. In this study, the degree of cell permeabilization (cell disintegration index) was directly measured by means of a new method using fluorescent dye propidium iodide (PI). The method allows for conclusions to be drawn about the effects of treatment time, electric field strength, and treatment temperature. Using a self-developed algorithm for image segmentation, disintegration of trichomes was observed over a period of 3 h. This revealed a direct correlation between cell disintegration index and decay of trichomes. This decay, in turn, could be brought into a direct temporal relationship with the release of phycocyanin. For the first time, this study reveals the relationship between permeabilization and the kinetics of particle decay and phycocyanin extraction, thus contributing to a deeper understanding of the release of cell metabolites in response to PEF. The results will facilitate the design of downstream processes to produce sustainable products from *Arthrospira platensis*.

Keywords: *Arthrospira platensis* (*Spirulina platensis*), pulsed electric field (PEF), cell disintegration, phycocyanin extraction, image segmentation, trichome decay, propidium iodide (PI) staining

OPEN ACCESS

Edited by:
Lutz Grossmann, University of Massachusetts Amherst, United States

Reviewed by:
Daniele Carullo, University of Milan, Italy
Michael Sandmann, Neubrandenburg University of Applied Sciences, Germany

***Correspondence:**
Justus Knappert
justus.knappert@tu-berlin.de

Specialty section:
This article was submitted to Sustainable Food Processing, a section of the journal Frontiers in Sustainable Food Systems

Received: *02 May 2022*
Accepted: *31 May 2022*
Published: *04 July 2022*

Citation:
Knappert J, Nolte J, Friese N, Yang Y, Lindenberger C, Rauh C and McHardy C (2022) Decay of Trichomes of Arthrospira platensis After Permeabilization Through Pulsed Electric Fields (PEFs) Causes the Release of Phycocyanin. Front. Sustain. Food Syst. 6:934552. doi: 10.3389/fsufs.2022.934552

INTRODUCTION

Due to climate change and the growing world population, which is projected to reach up to 10 billion people by 2050 (Abel et al., 2016), the food industry is confronted with huge challenges. Therefore, sustainable, high-quality protein sources are needed. Because the production of animal proteins greatly impacts the environment, vegetable proteins should be preferred for consumption (Nijdam et al., 2012; Poore and Nemecek, 2018). Besides conventional plant-based protein sources such as legumes, phototrophic microorganisms (i.e., microalgae and cyanobacteria) and other valuable cell metabolites have been investigated as a source of proteins (Becker, 2007; Grossmann et al., 2020). Compared to arable crops, culturing microalgae leads to an up to 10-fold biomass yield per area while the biomass is characterized by a similar or even higher protein content

(van Krimpen et al., 2013). Furthermore, microalgae can be cultivated on non-arable land or even on water surfaces (Kim et al., 2016). Among the many species available, *Arthrospira platensis (Spirulina platensis)* is a promising candidate as a novel protein source. This filamentous cyanobacterium is often mistakenly assigned to eucaryotic microalgae. One characteristic of *A. platensis* is the arrangement of cells in a helicoidal, cylindrical trichome. The cells are divided by cross cell walls, and their division leads to the elongation of the trichome (Tomaselli, 1997). The proliferation of trichomes is triggered by their breakage. *Arthrospira* can accumulate proteins by up to 70% of its biomass (Oliveira et al., 1999). In addition, protein from *A. platensis* is advantageous for human nutrition, since it contains all the essential amino acids (Becker, 2013). Recent studies revealed good techno-functional properties of cell proteins i.e., good emulsifying, foaming, and gel-forming capacity (Benelhadj et al., 2016; Bertsch et al., 2021; Böcker et al., 2021: Ramírez-Rodrigues et al., 2021).

One particularly valuable protein from *A. platensis* is the blue-pigment protein phycocyanin (PC). It belongs to the class of phycobiliproteins and acts as an accessory pigment in photosynthesis. Together with other phycobilins, allophycocyanin (APC), and phycoerythrin (PE), PC is located in phycobilisomes at the surface of the thylakoid membrane (Stadnichuk et al., 2015). It forms the major fraction of phycobilin proteins and can account for up to 20% of the biomass of *A. platensis* (Christaki et al., 2015). Several properties make PC a valuable molecule when extracted, increasing the overall value of the biomass. Recently, PC has received a lot of attention from the food industry, because it is one of the few natural blue food colorants (Sigurdson et al., 2017). PC shows thermal instability at temperatures $>50°C$ (Böcker et al., 2020), which restricts its use in foods. Nevertheless, in a high-sugar environment, the pigment has good thermal stability and is therefore particularly suitable for use in soft drinks and confectioneries (Martelli et al., 2014). In addition, various studies suggest that PC has anti-inflammatory, antiviral, and anti-cancer properties and that it can provide protection against diabetic nephropathy, making it interesting to the pharmaceutical industry (Shanab et al., 2012; Pleonsil et al., 2013; Zheng et al., 2013).

Despite great scientific and public interest in microalgae and cyanobacteria, the major commercial breakthrough has so far failed to materialize. This can be attributed to high production costs, particularly concerning cultivation and downstream processing. On the other hand, the market for *A. platensis* is relatively small, and it is mostly offered in the form of powder or tablets as a dietary supplement. One approach to overcoming this bottleneck is the implementation of biorefinery concepts. Similar to an oil refinery, the aim here is to process as many cell ingredients as possible into different products (Chew et al., 2017; Caporgno and Mathys, 2018; Carvalho et al., 2020). In the case of *A. platensis*, i.e., PC could be extracted and purified while the remaining cell protein could be offered at a reduced price for human consumption. For microalgae in general, it has been shown that this approach can raise the market price for a kilo of biomass from €.3 to around €30.5 (Ruiz et al., 2016). One crucial step for this approach is mild cell disruption, which increases the mass transfer of valuable cell metabolites across the cell membrane in order to separate them from the residual biomass.

A promising technology for the enhancement of mass transfer is the technology of pulsed electric fields (PEFs). This technology is based on the repeated application of high-energy electric fields ($kV\ cm^{-1}$) that are active for a very short time (µs or ns). During the pulse, spontaneously formed hydrophobic pores, grow and, above a certain pore size, become hydrophilic and thus permeable for various cellular substances (Saulis, 2010). A PEF has been recently investigated in the context of biorefinery approaches for different microalgae species (Buchmann and Mathys, 2019; Leonhardt et al., 2020; Papachristou et al., 2021; Carullo et al., 2022). Compared to other cell disruption methods such as bead milling, it was claimed that a PEF enables selective cell permeabilization for water-soluble substances while preserving cell structure (Goettel et al., 2013; Postma et al., 2016; Lam et al., 2017b). This in turn should enable facilitated separation of the cell debris after extraction of valuable substances of interest. Furthermore, the literature indicates that a PEF seems to be an energetically more efficient method for cell disruption in comparison to bead milling or ultrasound, as it enables the release of water-soluble metabolites at a lower or comparable specific energy input (Boer et al., 2012; Goettel et al., 2013; Postma et al., 2017; McHardy et al., 2021). However, in the context of process design, PEF technology requires a treatment medium with suitable electrical conductivity, which must fit the geometry of the treatment chamber used. on the one hand, high electrical conductivity leads to shorter pulse duration but to increased electric current and therefore to intensified heating during treatment on the other hand (Heinz et al., 2001). This could damage thermally sensitive valuables. Since standard culture media for *A. platensis* have an electrical conductivity of around $30\ mS\ cm^{-1}$(Aouir et al., 2015), direct treatment in these media is not possible. The aqueous phase must therefore be replaced, which can be expected to reduce economic efficiency on an industrial scale.

Concerning the treatment of *A. platensis* with PEF, several studies have shown that the technology is, in principle, suitable for permeabilizing the cell, thereby releasing compounds such as PC without extraction of water-insoluble components such as chlorophyll (Martínez et al., 2017; Jaeschke et al., 2019; Akaberi et al., 2020; Carullo et al., 2020; Käferböck et al., 2020). Even though flow cytometry and propidium iodide (PI) staining have been previously applied to detect the permeabilization of microalgae (Luengo et al., 2014; Knappert et al., 2020), they are not applicable to *A. platensis* because of the large size of the trichomes. Accordingly, the effect of PEFs on *Arthrospira platensis* was always determined indirectly in the cited studies by measuring the extraction kinetics for different molecules, i.e., PC, water-soluble proteins, or carbohydrates. A drawback of this approach to characterizing the impact of PEFs on cells is the time-consuming extraction process, which reduces the possible parameter sets to be investigated. Furthermore, conditions during the extraction process (e.g., temperature) have a direct impact on the extraction of the targeted molecule (Akaberi et al., 2020). This may bias statements regarding treatment efficiency and make it difficult to determine the true influence of PEFs

on cells. However, knowledge of cell disintegration efficiency is essential to design processes that ensure complete cell disruption while protecting the desired product from damage.

The mechanism underlying the release of the aforementioned molecules is also not conclusively clarified. For example, the cited studies differ greatly regarding the trend of PC extraction curves. While Martínez et al. reported that the extraction is preceded by a lag time of 150 min, Käferböck et al. (2020) reported the beginning of the extraction process right after PEF treatment. Jaeschke et al., on the other hand, observed a lag time depending on specific energy input. The studies contain contradictory statements regarding whether the preservation of cell morphology, observed for other microalgae, can be transferred to *A. platensis*. Jaeschke et al. reported in their study the decay of the trichomes over the extraction time for higher energy inputs (112 and 56 kJ l^{-1}) and only minor defects for the lowest energy input (28 kJ l^{-1}). In contrast, Martínez et al., Käferböck et al., and Carullo et al. stated that trichomes are predominantly preserved. However, none of these authors indicated the time after PEF treatment at which the size measurement occurred. A temporally resolved measurement is missing in all the four studies.

Based on the presented state of research, we hypothesize that the PEF treatment initially has no influence on the size of the particles. However, subsequent extraction over a period of several hours can lead to the disintegration of the trichomes, which in turn leads to the release of water-soluble cell metabolites such as PC. If this hypothesis was correct, the decay of trichomes would depend on treatment intensity, which could explain the different trends of the extraction curves presented in the literature. However, to separate the processes of cell permeabilization, trichome breakdown, and extraction, direct and uncoupled measures of all phenomena would be highly beneficial.

In order to test the hypothesis, we first developed a novel method to directly detect membrane permeabilization by staining *A. platensis* with the fluorescent dye propidium iodide (PI) and fluorescence spectrometry. With this method, the impact of PEFs on cells of *A. platensis* can be directly measured for the first time. This allows for an unbiased investigation of the effect of PEFs on cells without being affected by conditions during the extraction process, thus enabling a better understanding of parameter effects. Accordingly, we used the novel method to determine the effects of treatment time, electric field strength, and treatment temperature on the permeabilization of the cell membrane in the first series of experiments. The second part of this study addresses the question of whether PEFs trigger the decay of trichomes. Therefore, the particle size of trichomes or their fragments was monitored over a period of 3 h by light microscopy and digital image processing. Finally, we investigated whether the possible disintegration of trichomes is correlated temporally with the release of PC. The aim of this study is, thus, to gain a better understanding of the relationship between PEF process parameters and the mechanism for release of water-soluble contents from cells.

TABLE 1 | Medium composition used in this study for the SOT medium with original composition and reduced composition.

Solution	Substance	Original composition [g/L]	Reduced composition [g/L]
1	$NaHCO_3$	16.8	0.84
	K_2HPO_4	0.5	0.5
	Distilled water	500	500
2	$NaNO_3$	2.5	1.25
	K_2SO_4	1.0	0.5
	NaCl	1.0	0.5
	$MgSO_4 \times 7H_2O$	0.2	0.2
	$CaCl_2 \times 2\ H_2O$	0.04	0.04
	$FeSO_4$ * 7 H_2O	0.01	0.01
	Na_2EDTA * 2 H_2O	0.08	0.08
	A5	1.0	1.0
	Distilled water	500	500
Trace metal mix A5	H_3BO_3	0.286	0.286
	$MnSO_4$ * H_2O	0.15	0.15
	$CuSO_4$ * 5 H_2O	0.222	0.222
	Na_2MoO_4 * 2 H_2O	0.0079	0.0079
	Distilled water	100 ml	100 ml

MATERIALS AND METHODS

Arthrospira Platensis Cultivation

The cyanobacterium *Arthrospira platensis (Spirulina)*, strain NIES-39, was used in this study. The strain was kept in a 20-ml SOT medium (cf. **Table 1**) at room temperature and under constant illumination using fluorescent tubes with a light intensity of 20 μmol m^{-2} s^{-1} while being placed on a rotary shaker with a constant rotation frequency of 100 rpm. Light intensity was measured on the level of the medium surface inside the flask using a spherical micro quantum sensor and a light measuring device (ULM-500; Walz, Germany). Every 2 weeks, 1 ml of the culture was inoculated to a fresh medium.

To produce biomass for the experiments, *A. platensis* was cultivated in a bubble column photobioreactor with a culture volume of 1.4 l (reactor volume 1.65 l) and an inner diameter of 7 cm. Inline measurements of temperature (Biostream International, Netherlands) and pH (Hamilton, United States) were conducted using sensor probes, which were connected to a control unit with an integrated data logger (Biostream International, Netherlands).

The cultivation occurred in the reduced SOT medium. The composition of the reduced medium is shown in **Table 1** alongside the original SOT composition. The reduced medium was chosen in order to match the required electrical conductivity for the PEF treatment and reduce the required dilution factor after harvesting and concentrating the cells. Previous tests showed that cell growth in the reduced medium in terms of dry biomass was comparable to the one in the non-reduced medium (data not shown). For mixing, the bubble column was gassed with

air at a volume flow rate of 800 ml min^{-1} *via* a ring sparger. Because of the reduced amount of carbonate in the medium, its buffering capacity for the pH is limited. Therefore, the pH was automatically maintained by enriching the air with CO_2 using a CO_2 mass flow controller (Brooks Instrument, Germany) as soon as it rose above 9.5. To maintain the temperature at 30°C, the bubble column was placed in a water bath, which was tempered using an external heater. Continuous artificial white light was applied from two sides with LED panels (LED-Mg, Germany) with a total area of 0.171 m^2. Light intensity was set to 45 μmol m^{-2} s^{-1} measured at the surface of the bubble column with a light meter (ULM-500, Walz, Germany).

To determine the cell density of the culture, a correlation between biomass dry weight and optical density at 750 nm (OD_{750}) was established. The optical density of several diluted cell samples was measured in 1-cm cuvettes using a UV/VIS spectrometer (Lambda 25; Perkin Elmer). The cell dry weight of the same samples was determined by filtering them through pre-dried glass microfiber filters (Whatman GF/F, pore size 0.7 μm). The filters were washed two times with distilled water to remove salts and then dried for 24 h at 80°C. For each data point, cell dry weight and extinction were measured in triplicate. The resulting correlation was used to calculate the dry biomass of the sample.

The cells were harvested semi-continuously in the late exponential growth phase. To ensure this, specific growth rate was determined in a preliminary batch run (data not shown), and biomass concentration was determined ow times a day over the entire duration of the experiment. After harvesting, the culture was diluted with an autoclaved reduced SOT medium such that the biomass concentration had increased again to the same level the next day.

PEF Treatment

Sample Preparation

For sample preparation, the dry weight of the harvested cell culture needed to be adjusted to the intended concentration. This was conducted in two steps. First, the cells were separated from the growth medium and concentrated to a higher concentration than finally needed. Second, the concentrated cells were diluted and resuspended in a fresh SOT medium, which was previously adjusted to the desired electrical conductivity (2 mS cm^{-1}) by adding distilled water (hereafter termed as resuspension medium).

For this procedure, the dry weight biomass concentration of the culture was determined by spectrophotometry as described in Section PEF Treatment. The amount of cell culture needed for a certain amount of sample was calculated based on mass conservation; thus, $C_1 V_1 = C_2 V_2$, where $C_1$is the dry biomass concentration [g l^{-1}] measured inside the culture and $V_1$is the volume that must be harvested, C_2 is the desired dry biomass concentration (factor 1.6 higher concentration than finally needed), and V_2 is the desired sample volume. The cell culture was then filtered through microfilters (pluriStrainer 1 μm; pluriSelect Life Science, Germany) to separate the cells from the culture medium. The remaining pellet was rinsed with the same amount of distilled water to remove the salt. The pellet was transferred to a 50-ml Greiner tube by washing it off the filter with a fresh resuspension medium and filling the tube afterward up to 20 ml. The dry biomass concentration was again determined, and the required volume of the resuspension medium to reach the final concentration was calculated again according to $C_1 V_1 = C_2 V_2$. For experiments studying cell membrane permeabilization and trichome decay, the final biomass concentration was 1.5 g l^{-1}. For extraction of PC, the final biomass concentration was set to 5 g l^{-1}. The higher biomass for extraction was chosen to have a higher concentration of PC in the sample. This allows for a more accurate photometric measurement, as low concentrations are close to the blank value. For better comparability, the PEF treatment to measure particle decay was also performed at 5 gl^{-1} in this experiment.

Treatment Conditions

PEF treatments were performed in a prototype device designed in-house. The exact configuration is described elsewhere (Knappert et al., 2020). Voltage and electric current were directly measured in the treatment chamber by a 75-MHz high-voltage probe and a 100-MHz electric current probe, respectively. The measured signals were visualized and stored with a digital 200 MHz oscilloscope (TDS2022B; Tektronix, United States). Electroporation cuvettes (VWR) with a gap width of 4 mm and a volume of 800 μl served as treatment chambers. For temperature control during the experiment, the cuvettes and the PEF device were placed below a temperature-controlled incubator hood (Certomat, HK, Sartorius, Germany) for at least 30 min before each experiment. The sample was preheated for 15 min to reach the desired temperature using a thermomixer (Hettich Benelux B.V., Netherlands) by shaking at 300 rpm.

In the first series of the experiments, the effect of electric field strength, initial treatment temperature, and treatment time were investigated. The applied treatment conditions are summarized in **Table 2**. Exponential pulses were applied with a time constant of 2 ± .63 μs and a pulse repetition rate $f = 1$ Hz. The pulse counts (number of applied pulses) for the various treatment conditions were selected such that the critical parts of the expected curve for cell permeabilization can be well-represented. These are, namely, parts where cell disintegration rises and reaches a plateau. After the treatment, each sample was diluted to a suitable concentration for the following measurements (cell membrane permeabilization for PI and particle size decay, see following paragraphs) by transferring the treated sample to an ice-cooled resuspension medium. The samples were stored on ice until further analysis.

The specific energy input w_{spec} of the treatment was calculated as follows:

$$w_{spec} = \frac{1}{m} n_p \int_0^{f^{-1}} U(t)\ I(t)\, dt \tag{1}$$

where m is the mass of the sample (800 μg, estimated density = 1 g cm^{-3}), n_p is the number of applied pulses, and $U(t)$ and $I(t)$ stand for voltage and electric current, respectively.

TABLE 2 | Number of pulses applied to the sample for different pulsed electric field (PEF) treatments.

	Initial treatment temperature [°C]		
Electric field strength [kV cm^{-1}]	**30**	**40**	**50**
5	6, 24, 40, 55, 65, 80, 90, 120	6, 24, 40, 55, 65, 80, 90, 120	6, 24, 40, 55, 65, 80, 90, 120
10	1, 6, 12, 24, 40, 55, 65, 70	1 ,6, 12, 24, 32, 40, 55, 65	1 ,6, 12, 24, 32, 40, 55, 65
15	1, 3, 6, 12, 24, 32, 40, 50, 60	1, 3, 6, 12, 24, 32, 40, 50, 60	1, 3, 6, 12, 24, 32, 45, 60
20	1, 2, 3, 6, 12, 24, 32, 40	1, 2, 3, 6, 9, 12, 18, 24, 32	1, 2, 3, 6, 9, 12, 18, 24, 32
25	1, 2, 3, 6, 12, 18, 24, 32	1, 2, 3, 6, 12, 18, 24, 28, 32	1, 2, 3, 6, 9, 12, 18, 24, 32

Analytical Methods

Measurement of Cell Permeabilization

To detect the effect of PEFs on permeabilization of the cell membrane, a novel method based on fluorescence spectrometry was developed in-house. PI, a substance that cannot penetrate intact lipid membranes, was used as a dye. This substance has already been used as a dye to detect cell disintegration of phototrophic microorganisms (Luengo et al., 2014; Knappert et al., 2020). For the development of the method, heat-inactivated cells were used (80°C, 15 min) to minimize pigment interference with PI. The parameters biomass concentration, PI concentration, staining time, and staining temperature were varied based on experimental designs. After the optimal staining parameters were found, the excitation and emission wavelengths were adapted in order to measure samples with high pigment content (i.e., PEF-treated samples). For a more detailed description of the method development, refer to **Appendix A**. Fluorescence measurements were conducted using a fluorescence spectrofluorometer (RF-6000; Shimadzu, Japan).

The final method consists of the following steps. First, a PEF-treated sample was diluted using an ice-cooled resuspension medium to a biomass concentration of $C_B = 0.25$ g l^{-1}, and 1.8 ml of the diluted sample was mixed with 200 µl PI stock solution. The final PI concentration in the sample was $c_{PI} = 11.2$ µg ml^{-1}. One unstained sample per treatment was prepared to check whether cellular autofluorescence was affected by the treatment, which was not the case for all the treatment conditions (data not shown). The samples were shaken using a thermomixer (Hettich Benelux B.V., Netherlands) at 23.1°C and 300 rpm for 17.5 min. After incubation, the sample was transferred to a quartz cuvette (Helma Analytics, No. 101-10-40, Germany) and measured directly at an emission wavelength of 580 nm (bandwidth 5 nm) and an excitation wavelength of 490 nm (bandwidth 5 nm).

The degree of cell permeabilization was characterized by the cell disintegration index Z_D as defined in Lebovka et al. (2002):

$$Z_D = \frac{Z - Z_0}{Z_m - Z_0} \tag{2}$$

Here, Z is the measured fluorescence signal, Z_0 is the fluorescence signal of the untreated sample, and Z_m is the maximum fluorescence signal at complete cell disintegration. To obtain Z_m, reference treatment conditions were defined in pretrials at which the fluorescence signal reached its maximum. Here, 25 kV cm^{-1} and 32 pulses were chosen as reference treatment conditions at a given temperature (cf. **Table 2**). These parameters were validated by trying to recultivate the treated cells in a fresh full SOT medium. After 3 days, the cells were agglomerated and started to bleach out, and no growth occurred. Therefore, these treatment conditions were considered to cause full irreversible membrane permeabilization.

For all the treatment conditions (**Table 2**), the cell disintegration index was determined in two biological replicates and two technical replicates of the PEF treatment. Three technical replicates were conducted for the reference treatment and the untreated sample. The staining of each sample was conducted in duplicate. Before calculating Z_D, the arithmetic mean of all four or six stained samples was calculated for each biological repetition and inserted into Equation 2 for Z, Z_0, and Z_m, respectively. For each treatment condition, we report the arithmetic average of the two biological repetitions and corresponding standard deviations.

Measurement of Cell Size Distribution

An analysis of cell size distribution after treatment was performed using microscope images and a self-developed image segmentation algorithm. Cells were treated with the parameter combinations listed in **Table 2**, with the highest applied pulse repetition number. Directly after the treatment, the treated sample was diluted to a dry biomass concentration of to $C_B = 0.25$ g l^{-1} ($OD_{750} = 0.5$). RGB images were taken using a light microscope (Primo Star; Zeiss, Germany, 40× magnification), equipped with a digital camera (Digital Sight DS-U3; Nikon). The treated cell samples were tempered at 30°C in a thermomixer at 300 rpm. After 0, 30, 60, 120, and 180 min, a sample was taken, and microscopic images of the cells were taken. At least 700 cells were detected (untreated sample, 180 min). Additionally, an untreated and a treated sample were kept at 30°C without shaking to investigate if the shaking itself has any impact on cell size distribution. For image acquisition, a sample was transferred to a counting chamber (Thoma counting chamber; Hecht Assistant, Germany) and covered with an optical cover glass. A total of 20 images were taken for each PEF treatment and time at which samples were taken (0, 30, 60, 120, and 180 minutes).

The obtained images were processed using the commercial software MATLABR2021a. The image processing code can be obtained upon request to the corresponding author. The algorithm is schematically shown in **Figure 1**. First, an RGB image was converted into a grayscale. Then, the image was smoothed using a Gaussian filter, and the contrast was enhanced based on the standard deviation of the gray values. After background subtraction, the image was converted into a binary image. For this, we first selected upper and lower thresholds based on grayscale histogram values to create two binaries, A and B, of which we computed the intersection A∩(¬B). Objects

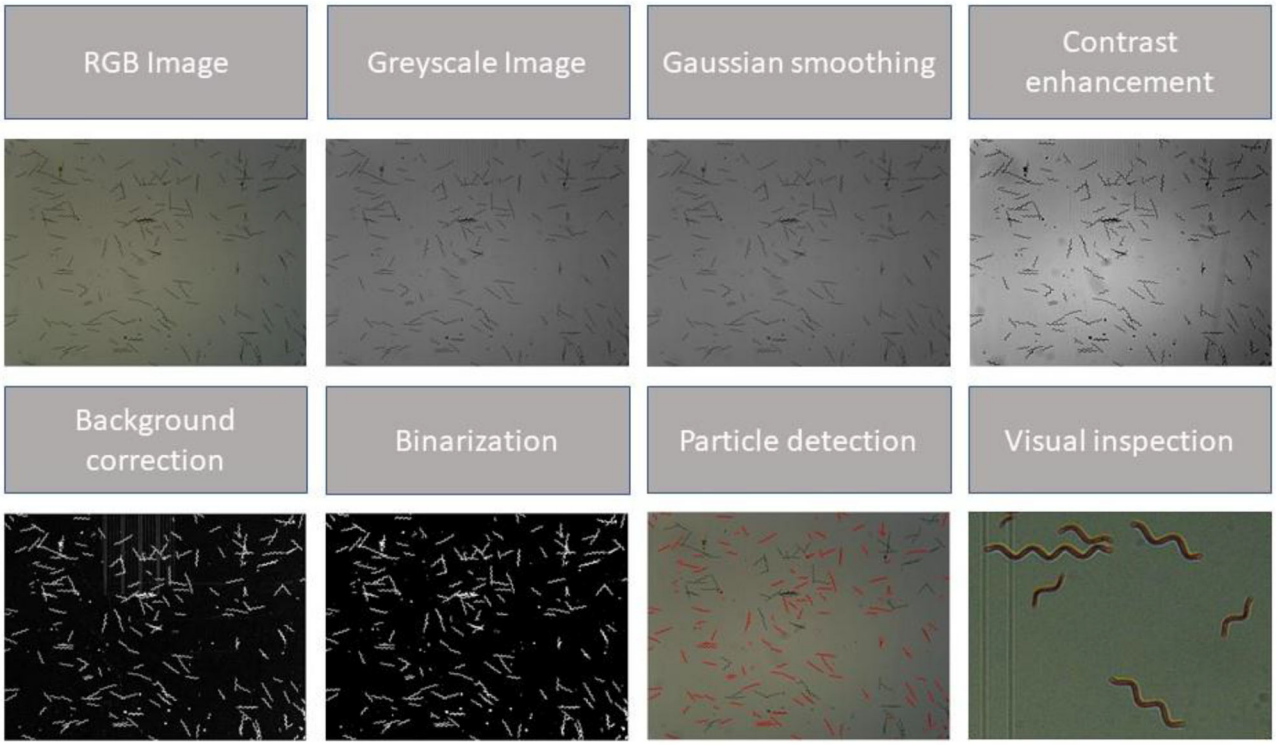

FIGURE 1 | Concept of the proposed image processing algorithm. From top left to bottom right: The (RGB) image was loaded and converted into a grayscale image. The image was smoothed by applying a Gaussian filter, and the contrast was enhanced. The background was subtracted, and the picture was binarized. Particle detection was performed by filtering the detected particles based on their region properties. Edge detection and particle detection were inspected visually, and parameters were adapted if the result was inconvenient. Note that border clearing and filling of smaller holes are not presented in this scheme.

on the edges of an image were cleared out, and small holes ($\leq$4 pixels) in objects were filled. The received objects represented the cells and were assigned to different size classes based on the region properties area, circularity, eccentricity, solidity, minor axis length, and major axis length. To distinguish between cells and dirt or other impurities, five size classes were created with different values for the named region properties. The values for the classes are listed in **Table 3**. To calibrate the pixel-to-length ratio, the defined grid of the Thoma chamber was used. The pixels between the grid lines were counted manually, allowing for the length to be calibrated by the known grid spacing.

To determine the accuracy of the method, the sensitivity of the algorithm was determined for each class. Six images representative of field strength, time, and temperature were randomly selected from the entire pool of images. The objects in each class were manually counted and visually inspected to determine whether a detected object is an *A. platensis* trichome or a fragment. The sensitivity *S* is calculated as:

$$S = \frac{r_p}{r_p + f_n} \tag{3}$$

where r_p is the correctly recognized cells (true positive) and f_n is the incorrectly unrecognized cells (false negative). As a second parameter, the false positive rate *F* was calculated according to:

$$F = \frac{f_p}{r_n + f_p} \tag{4}$$

where r_n is the number of objects that were correctly not recognized as cells (true negative) and f_p is the number of objects that were falsely recognized as cells (false positive). The results of the accuracy tests are listed in **Table 3**. The standard deviations given in the **Table 3** are calculated from the differences in the calculated values for S or F for the six selected images.

Extraction and Measurement of Phycocyanin

For PC extraction, the sample was prepared as described in Section Sample Preparation except that the pH of the sample was adjusted to 6 using 2 M HCl. The extraction was conducted in the dark using a thermomixer at 30°C and 700 rpm. Samples were taken after 0, 30, 60, 120, 180, and 240 min for the analysis of the concentration of the extracted PC; 60 µl of each sample was taken and diluted with a resuspension buffer for particle size measurement (see Section Measurement of Cell Size Distribution). The samples were centrifuged at 12,000 *g* for 5 min. The supernatant was transferred to a quartz cuvette (Helma Makro-Cuvette 100-QS). The concentration of phycocyanin *PC* was determined spectrophotometrically and calculated according

TABLE 3 | Size classes for particle detection based on the pixels of the area region property.

	Region property area [pixels]				
	10–100	**100–800**	**800–1,800**	**1,800–5,000**	**5,000–7,000**
Circularity	-	0.01<x <0.55	0.01<x <0.55	0.05<x<0.3	0.05<x<0.1
Eccentricity	-	0.5<x<0.998	0.7<x<0.999	0.8<x<0.998	0.98<x<0.999
Major axis length	-	-	-	-	<6,000
Minor axis length		<60	<55	<40	<50
Solidity	-	-	-	<0.645	<0.65
Sensitivity S	0.932 (0.02)	0.944 (0.11)	0.912 (0.31)	0.91 (0.38)	
False positive rate F	0.624 (0.22)	0.516 (0.19)	0.340 (0.26)	0.13 (0.10)	

The values in parentheses represent the standard deviation for the sensitivity S and the false positive rate F, respectively.

to the following equation (Bennett and Bogorad, 1973):

$$PC\ [mg\ ml^{-1}] = \frac{OD_{615} - 0.474 OD_{652}}{5.34} \tag{5}$$

Here, OD_{615} and OD_{652} are the optical densities over a light path of 1 cm at 615 and 652 nm, respectively. The extract purity *EP* was obtained spectrophotometrically and calculated as (Abalde et al., 1998):

$$EP = \frac{OD_{615}}{OD_{280}} \tag{6}$$

where OD_{250} is the optical density at 250 nm. Since this experiment was performed to test the hypothesis that extraction yield is correlated with the decline of the average particle size, it was only conducted for one set of treatment conditions, which led to full membrane permeabilization, and for one which led to permeabilization of 50% (see Section Impact of PEFs on Average Particle Size).

Ultrasound Treatment

Ultrasound treatment was performed as a reference method using a Sonopuls UW70 ultrasound processor and a SH70 sonotrode (Bandelin, Germany). The power input at a setpoint of 100% is 60 W. For the treatment, 10 ml of liquid with a biomass concentration of 2.5 g l^{-1} and a pH of 6 was transferred to a Greiner tube and repeatedly treated over five cycles, where one cycle consisted of 10 s of treatment and 20 s of cooling in an ice bath. The lower biomass concentration of 2.5 gl^{-1} (compared to 5 gl^{-1}) was chosen to avoid excessive dilution throughout the semi-continuous cultivation process. During the method development, higher biomass concentrations were tested, and no difference was observed with respect to the extractability of PC (data not shown). After the treatment, the Greiner tube was shaken in the dark at 700 rpm. Samples were taken after 0, 30, 60, 120, 180, and 240 min for particle size measurement (cf. Section Measurement of Cell Size Distribution) and for phycocyanin measurement (cf. Section Extraction and Measurement of Phycocyanin).

RESULTS AND DISCUSSION

Effect of PEF on *Arthrospira platensis* Cells

Experimental Results

The influence of the PEF treatment in terms of the cell disintegration index $Z_D$was analyzed with respect to treatment time as well as electric field strength and treatment temperature. The results obtained by PI staining and fluorescence spectroscopy are shown in **Figure 2**. The treatment time is calculated as the product of the number of applied pulses and the time duration of each pulse. It can be concluded that the different treatment parameters influence the permeability of the cell membrane for PI to different extents. For all the three treatment temperatures, an electric field strength equal to or >15 kV cm^{-1} was sufficient to permeabilize all cells. At lower electric field strengths, a plateau value of $Z_D < 1$ was reached after the longest treatment time. Furthermore, an interaction between electric field strength and treatment temperature was observed, which influenced the trend of Z_D. For example, no increase in Z_D was observed at the lowest electric field strength (5 kV cm^{-1}) and 30°C, while at the same field strength, it increased by up to 0.376 and 0.633 at 40 and 45°C, respectively. Similar trends were observed for the treatment at 10 kV cm^{-1}. While the treatment at 30 and 40°C did not lead to full permeabilization ($Z_D = 0.556$ and 0.826), this was the case for the treatment at 45°C.

The treatment temperature also has a strong influence on the trend of Z_D at electric field strengths that led to complete permeabilization. Thus, a longer treatment time was required to achieve this at 30°C compared to treatments at 40 or 45°C. To clarify this, the treatment time required to achieve complete permeabilization of the cells is shown in **Figure 3**. The time for full permeabilization is calculated as the arithmetic mean from the two biological repetitions, and the corresponding standard deviation from the two samples is shown. At 30°C and 15 kV cm^{-1}, 122 µs was required to complete the permeabilization, whereas the time was reduced by about half at 45°C (50.8 µs). This trend is also confirmed at higher field strengths. The difference between treatments at 20 and 25 kV cm^{-1} is more pronounced at temperatures of 30 and 40°C, respectively, while the error bars overlap strongly at 45°C. This behavior is evident over the entire course of the treatment time at the two highest electric field strengths (cf. **Figure 2**). This result indicates that

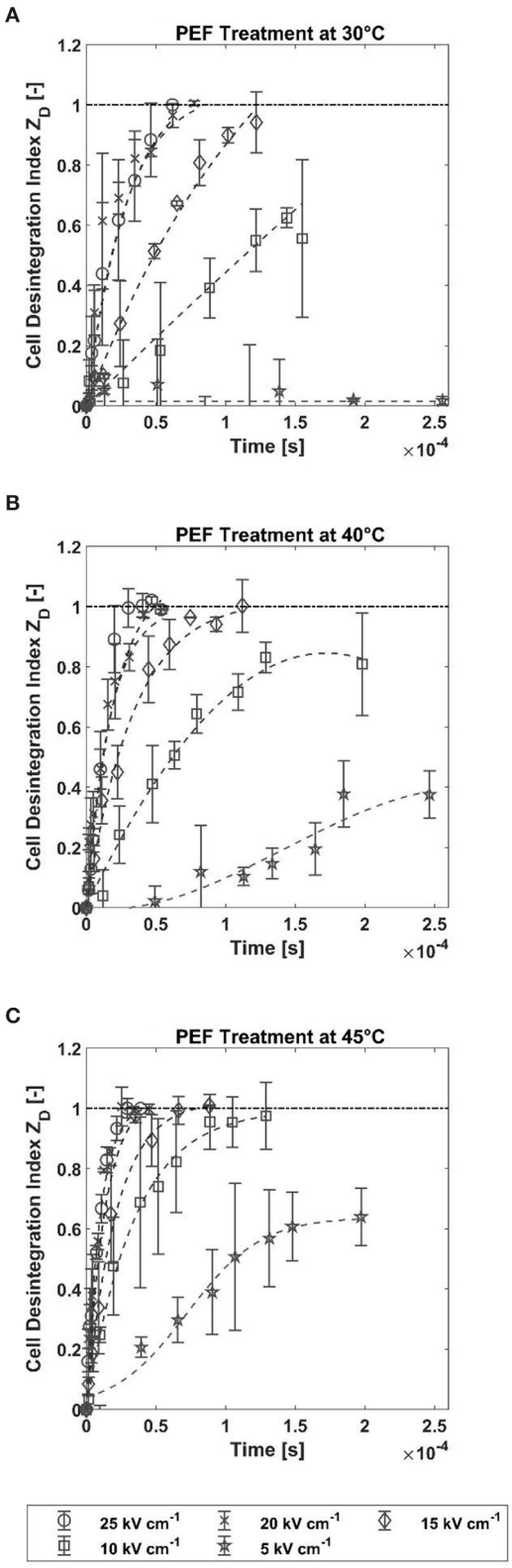

FIGURE 2 | Cell disintegration index Z_D vs. treatment time at five different field strengths and treatment temperatures of 30, 40, and 45°C. The error bars represent the standard deviation between mean values of the two biological repetitions (each calculated from the average of at least 4 values). The dashed dotted lines represent the best fits with polynomial models as an aid to the reader's eye and do not represent a mechanistic model. **(A)** PEF treatment at 30°C. **(B)** PEF treatment at 40°C. **(C)** PEF treatment at 45°C.

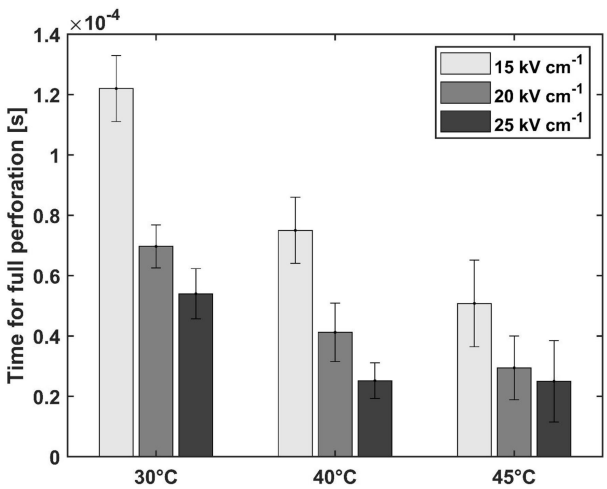

FIGURE 3 | Treatment time needed for full perforation ($Z_D = 1$) at electric field strengths that led to full permeabilization at all treatment temperatures. The error bars represent the standard deviation between two biological repetitions (repetition of the measurement on 2 days).

increasing the electric field strength from 20 to 25 kV cm^{-1} does not have an effect on permeabilization of the cell membrane of *A. platensis*. A possible explanation for this is the coarse resolution of the curves in terms of treatment time. Therefore, it cannot be concluded from the data whether the treatment at 25 kV cm^{-1} may have caused full permeabilization in a shorter treatment time. To evaluate the influence of the factors temperature and field strength on the critical treatment time more accurately, a two-factor ANOVA was performed using the data analysis tool in Excel. The test variable F was above the critical F-value (4.25 each) for both temperature (21.8) and field strength (19.53). The significant effect of the two variables on treatment time is also confirmed by the *p*-value of 0.00035 and 0.00053, respectively (at a 5% error probability). However, no significant influence could be found for the interaction of the factors temperature and field strength (*F*-value 1.26, critical *F*-value 3.63, and *p*-value 0.34). However, it should be mentioned that the temporal resolution of the experiment is relatively coarse because of the applied number of pulses. With two biological replications, the number of measurements is also relatively small (two mean values from one biological repetition each), which limits the statistical significance.

The interaction between treatment temperature and electric field strength makes it possible to control the process by these parameters. This increases the number of degrees of freedom in process design. If, for example, waste heat from another process is available, it can be used to save electrical energy. The natural

limits determined by the temperature tolerance of the product should be considered here. For example, PC starts to degenerate at a temperature of ∼50°C (Böcker et al., 2020). However, the results also indicate that the adjustment of electric field strength is only possible to a limited extent. As previously mentioned, the curves of Z_D without complete perforation converge toward a plateau (cf. **Figure 2**). This implies that full disintegration at electric field strengths below a critical value is not possible solely by extending the treatment time, which again is dependent on the treatment temperature. This result conforms with the results of our previous study, where similar plateaus were observed for the microalga *Chlorella vulgaris* (Knappert et al., 2020). Pataro et al. (2011) also measured a similar behavior for the yeast *Saccharomyces cerevisiae*. The observed relationships can be explained by the critical transmembrane potential that must be exceeded for irreversible pores to form, which depends, among other things, on cell size (Saulis, 2010). Since cell size is always distributed in a cell population, this potential may not have been exceeded for all cells.

Comparison to Literature Data

Since measurement of the cell disintegration index of *A. platensis* using PI has never been conducted before, a direct comparison to the data available in the literature is difficult. For better comparability, the specific energy input for the treatment was calculated according to Equation 1. The results of the calculation are shown in **Figure 4**. Despite some scattering in the data, the cell disintegration index follows a trend, and the slope of the curve depends on the treatment temperature. While 46.5 kJ kg^{-1} was required at 30°C to permeabilize all cells for PI, the specific energy input was almost halved to 25 and 21.8 kJ kg^{-1} at 40 and 45°C, respectively. Because of the variations in specific energy input between treatment intensities and relatively small differences in the electric field strengths at which complete permeabilization is reached, it is not possible to infer from the data whether a lower energy input is required for complete permeabilization at higher field strength. Therefore, the indicated energy inputs for full permeabilization should be only understood as an order of magnitude estimate. Nevertheless, **Figure 4** shows that the increase in Z_D is initially independent of the electric field strength. The samples differ only in their maximum value, which, as already described, is a function of the electric field strength and the treatment temperature (cf. **Figure 2**).

Carullo et al. (2020) treated cells from *A. platensis* with monopolar, rectangular pulses at 25°C and three different specific energy inputs, namely, 20, 60, and 100 kJ kg^{-1}. The effect on the cells was determined by total water-soluble protein content. The results of this study show an increase in extracted water-soluble proteins with increasing specific energy input and electric field strength. Similar behavior was also observed in this study. An increase in field strength and specific energy input was accompanied by an increase in the degree of permeabilization. In the same study, the influence of treatment temperature on the extractability of PC was also measured at a constant energy input (100 kJ kg^{-1}). It was found that treatment at 25°C resulted in significantly lower extraction yield compared to treatments at 35 and 45°C. Since heating in a continuous mode occurs differently

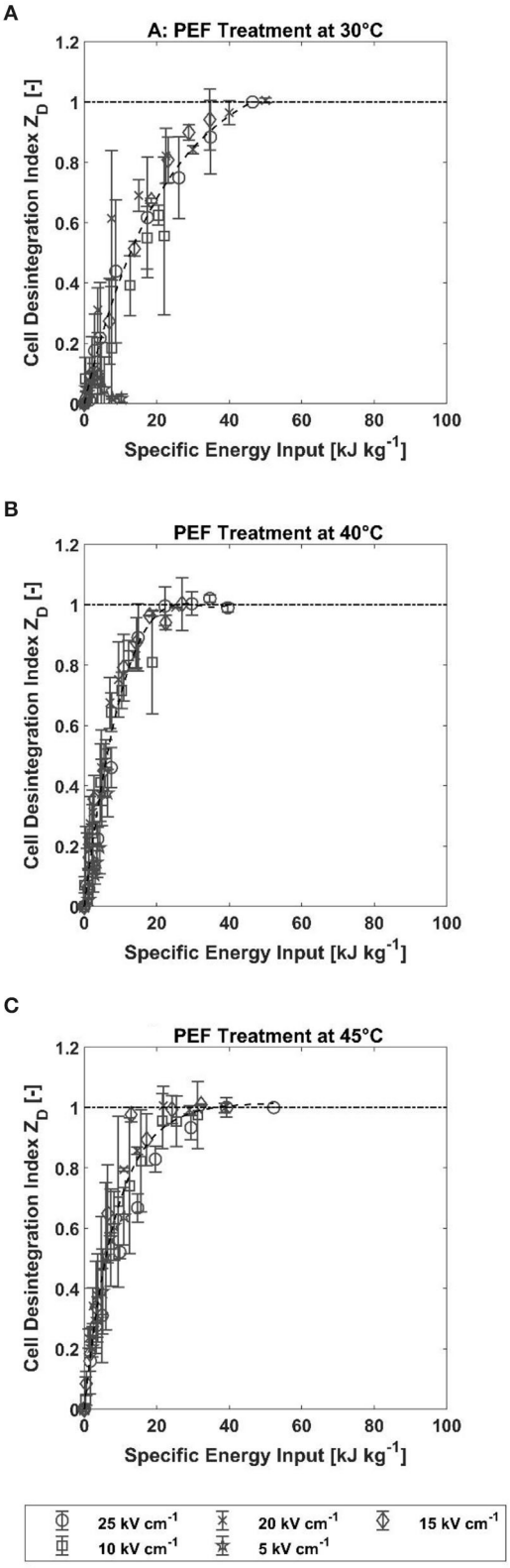

FIGURE 4 | Cell disintegration index Z_D as a function of electrical energy input for treatment temperature of 30, 40, and 45°C. The error bars indicate the standard deviation between the mean values of two independent measurements. **(A)** PEF treatment at 30°C. **(B)** PEF treatment at 40°C. **(C)** PEF treatment at 45°C.

than in a batch cuvette, the results cannot be compared directly to this study. However, our study also shows that the largest difference with regard to cell permeabilization was between the lowest (30°C) and the two highest temperatures (40 and 45°C), which conforms with the results of the study by Carullo et al. In contrast, Jaeschke et al. (2019) found no difference in PC yield obtained with specific energy inputs of 56 and112 kJ kg^{-1}.Specific energy input of 56 kJ kg^{-1} is in the same order of magnitude as the necessary energy input for the full permeabilization we have found in this study at a treatment temperature of 30°C (46.5 kJ kg^{-1}).

The two cited studies show that the trends for the measured permeabilization in this study are generally in agreement with literature data for the extraction of water-soluble proteins and PC. However, there are differences in the absolute values for the specific energy input that was necessary for full permeabilization in our study and full protein release in the studies by Carullo et al. and Jaeschke et al.. This can be explained by the different electric field strengths applied, treatment temperatures, and treatment cells (batch vs. continuous). Furthermore, it should not be directly deduced from the presented results whether complete permeabilization for PI is also correlated with the extraction yield of water-soluble protein or PC. The literature reports that treatment intensity has an influence on the permeability of the cell membrane for molecules of different sizes. Thus, the cell membrane becomes permeable to larger molecules only at higher field strengths, while smaller molecules can already leave after cells have been treated at lower intensities (Saulis, 2010). Various studies with other microalgae have already shown that small molecules such as carbohydrates can be extracted but that larger molecules such as proteins might stay inside cells (Postma et al., 2016; Lam et al., 2017a; Pataro et al., 2017; Carullo et al., 2018). Furthermore, PC is localized in the thylakoid membrane of the chloroplast from which it must be first dissolved. This may require higher treatment intensity than permeabilization of the membrane for PI.

Impact of PEFs on Average Particle Size

Temporal Evolution of the Average Particle Size

In agreement with the literature, the measured average major axis length of *A. platensis* trichomes remained unaffected immediately after the PEF treatment. This is illustrated for the treatment at 10 kV cm^{-1} and 45°C as an example in **Figure 5**. However, it is clearly observable that the trichomes start to disintegrate after 30–60 min. Visually, no difference can be seen between the images taken at 60, 120, and 180 min, since most of the trichomes have already completely decayed to smaller particles. The images shown prove for the first time that PEFs lead to a time-delayed decay of the trichomes of *A. platensis*.

For a quantitative analysis of this observation, the average length of the major axis of all detected trichomes was evaluated, which we hereafter term as average particle size. It must be recalled that the experiments in this study were carried out on different days. As a result, the growth phase at harvest may have deviated slightly, which would also affect the particle size distribution of the harvested biomass. Accordingly, the average particle size at 0 min after the PEF treatment was found in the range of 80–110 μm, which is in close agreement with the literature (Tomaselli, 1997). However, a direct comparison between single experiments becomes difficult because of the variation in average particle size between different days. To achieve comparable results, the relative length variation (RLV) is introduced, which is expressed as the ratio of the average particle size L at time t and 0 min (t_0):

$$RLV = \frac{L_t}{L_{t_0}} \tag{7}$$

The RLV is shown in **Figure 6** for all the treatment conditions tested. Independently of the temperatures, the untreated samples did not show any remarkable decrease in the average particle size over the observation time of 180 min. Since all the samples were tempered at 300 rpm for 15 min before treatment, it can be concluded that this process alone does not affect the average particle size. For an electric field strength of 5 kV cm^{-1}, the treatment did not show an effect on the samples at 30 and 40°C, whereas a slight decrease to 84% occurred after treating at 45°C. This observation is partially in line with the results from section 3.1. While no increase in the cell disintegration index Z_D was measured at 30°C, an increase was detected at higher temperatures.

At a temperature of 30°C and electric field strengths between 10 and 25 kV cm^{-1}, the decay of the average particle size depends on the electric field strength and time. If the electric field strength was higher than 10 kV cm^{-1}, a decrease in the average particle size was detected after 30 min, but no difference was found with respect to electric field strengths. After 60 min, the RLV becomes inversely proportional to electric field strength, i.e., the largest decrease was measured for the highest electric field strength (RLV = 0.45 for 25 kV cm^{-1}, 0.68 for 20 kV cm^{-1}, and 0.82 for 15 kV cm^{-1}). In contrast, treatment at 10 kV cm^{-1} had no measurable effect on the average particle size after 60 min of incubation. After 120 min, the samples treated with an electric field strength $\geq$ 15 kV cm^{-1} reached the minimum RLV of 0.23, which corresponds to an absolute average particle size of 21.59 μm (± 1.49 μm). Since the temporal resolution is very coarse, it cannot be concluded from the available data whether this minimum is reached between 60 and 120 min independent of the electric field strength. The samples treated at 10 kV cm^{-1} did not reach a steady RLV within the investigated incubation time. For this treatment, the decrease in average particle size started after 60 min and decreased to an RLV of 0.43 after 180 min. This matches very closely with the results presented in Section Effect of PEF on *Arthrospira platensis* Cells in which ∼55% of the cells were affected by the treatment under the same conditions.

At temperatures of 40 and 45°C, all the treatments at electric field strength >5 kV cm^{-1} led to complete disintegration of the particles within 180 min. However, the temperature affects the lag time after which the decrease starts. While the decay starts after 30 min at a temperature of 40°C (except for an outlier for 15 kV cm^{-1}), a treatment temperature of 45°C results in an earlier start of the disintegration process. For treatments with electric field strengths of 20 and 25 kV cm^{-1}, almost all cells are disintegrated after 30 min (RLV = 0.31). In contrast, for electric field strengths

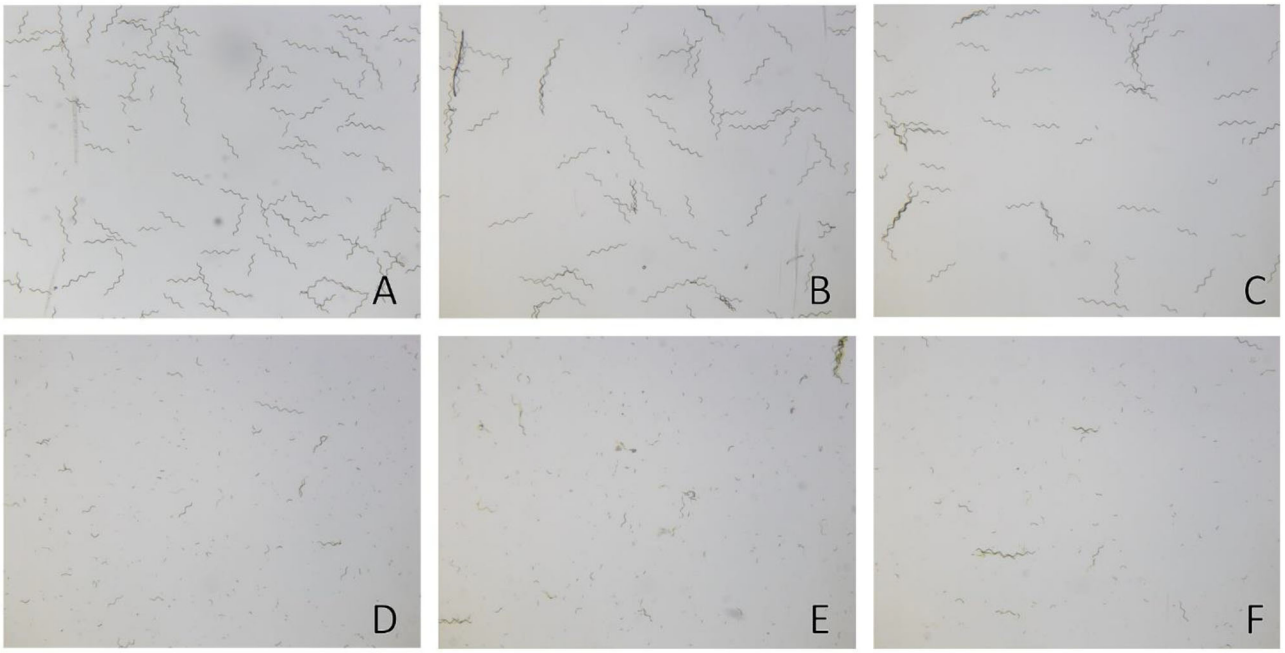

FIGURE 5 | Decay of *Arthrospira platensis* trichomes over time after pulsed electric field (PEF) treatment, shown for the treatment at 10 kV cm^{-1} and 45°C as an example. **(A)** Untreated cells. **(B)** PEF-treated cells after 0 min. **(C)** PEF-treated cells after 30 min. **(D)** PEF-treated cells after 60 min. **(E)** PEF-treated cells after 120 min. **(F)** PEF-treated cells after 180 min of incubation.

of 10 and 15 kV cm^{-1}, cell disintegration depends on the electric field strength.

In summary, the disintegration of the particles is consistent with the measured permeability for PI (refer to Section Effect of PEF on *Arthrospira platensis* Cells). In other words, the treatment parameters that led to a complete staining of the cells with PI also cause a complete decay of the average particle size toward a stationary value of the RLV. This statement can be supported by comparison with the microscopic images, where only a few intact trichomes can be observed after 180 min (see **Figure 5F**). Since the arithmetic mean is sensitive to outliers, the remaining trichomes, in combination with falsely detected contaminations, may be the reason why the RLV does not decrease to a lower value, although visually almost all the trichomes have decayed (minimum RLV = 0.2).

Comparison to Literature Data

Since no data on the particle size evolution of *A. platensis* trichomes after PEF treatment have been ever published, a direct comparison of our results with the literature is not possible. Nevertheless, the curves of the average particle size shown in **Figure 6** are strongly reminiscent of the published extraction kinetics for various substances such as PC or water-soluble proteins. Martínez et al. (2017) showed a clear time- and field strength-dependent release of phycocyanin, which is inversely proportional to the presented decay of the average particle size. Martínez et al. investigated the release of PC for two treatment times (specific energy input levels), namely, 75 and 150 µs. For the shorter treatment, a PC yield of around 100 mg g^{-1} dry weight was obtained at an electric field strength of 25 kV cm^{-1} and 60 mg g^{-1} at 20 kV cm^{-1}. Compared to the untreated sample, only a small amount of PC was released at 15 and 10 kV cm^{-1}. For the longer treatment (150 µs), treatments at 25 and 20 kV cm^{-1} led to a similar result, whereas for treatment at 15 kV cm^{-1} no stationary PC yield was reached within the investigated extraction time. Remarkably, they observed a lag time of around 150 min until an increase in PC concentration in the extract was detectable. While the observed lag time was independent of the applied electric field strength, their data do not allow for conclusions about its temperature dependency. Observing the decay in the average particle size, we found a dependency of the lag time on both electric field strength and temperature. Moreover, the observed lag time is shorter than that reported by Martínez et al., which might be because of the use of different strains or the slightly higher treatment temperature in our case. Furthermore, the specific energy input was also different (this study: 46.5 kJ kg^{-1}, in Martínez et al.: 93.7 kJ kg^{-1}).

Jaeschke et al. (2019) treated their samples in a continuous small-scale flow chamber (3 ml min^{-1}) at 40 kV cm^{-1} and three different pulse repetition rates, resulting in three levels of specific energy input (112, 56, and 28 kJ l^{-1}). At the highest level of specific energy input, no lag time for the release of PC was observed, while at the two lower levels, the release of PC started after a lag time of around 30 min. The authors compared their study to Martínez et al. (2017) and explained the

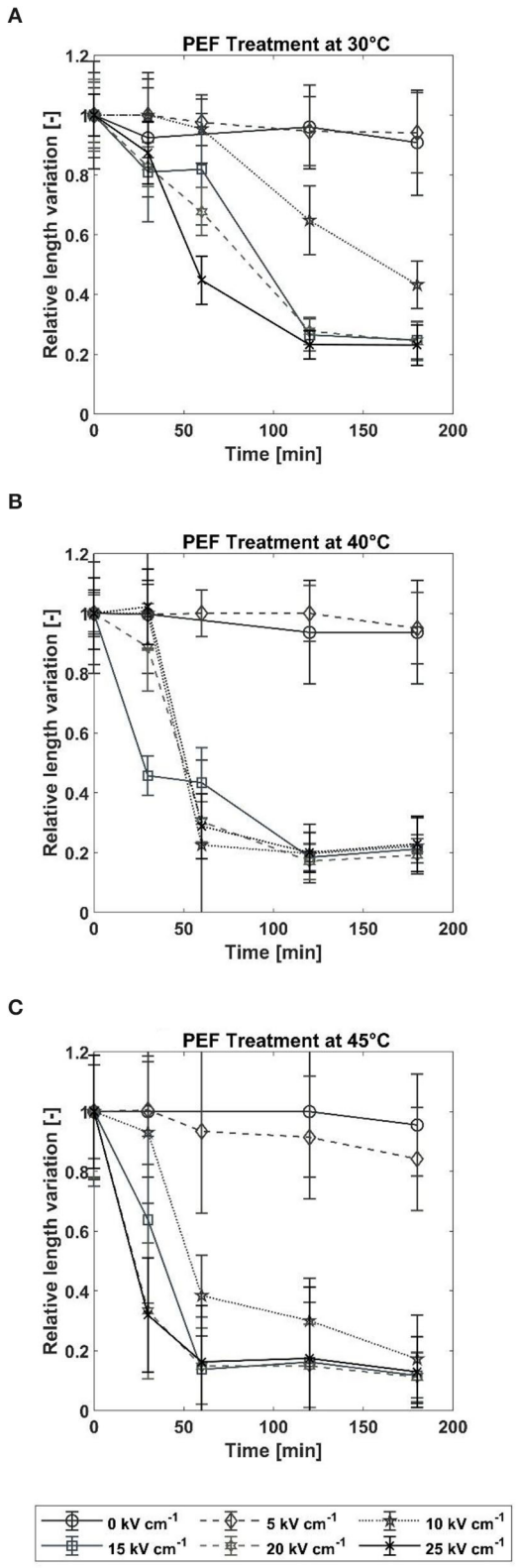

FIGURE 6 | Relative change in average particle size after PEF treatment at **(A)** 30°C, **(B)** 40°C, and **(C)** 45°C. The error bars show the deviations of the detected particles from the mean value and thus represent the width of particle size distribution.

different lag times based on the application of a higher electric field strength. This fits with our results for the decay in the average particle size, since, e.g., at a treatment temperature of 30°C, we measured the dependence of decay rate on electric field strength (refer to **Figure 6A**). Jaeschke et al. (2019) treated their samples at room temperature (25°C) but reported a temperature increase of up to 42°C during the treatment. Since our results indicate that lag time is also a function of temperature, this may also explain some of the differences with the results of Martínez et al. (2017), who treated their samples at 25°C in a temperature-controlled treatment chamber. After separating the extract, Jaeschke et al. (2019) also investigated the particle size in the pellet using a light microscope. The authors reported damage of trichomes for the two higher specific energy input levels, while the trichomes were less disintegrated at the lowest energy input. However, their study provides only a qualitative observation, and not the systematic evaluation that this study does.

Based on particle size analysis as well as light and electron scanning microscopy, Carullo et al. (2021) stated that mean particle size does not change after PEF treatment. However, they did not specify the time at which the images were taken after the treatment. Assuming that the images were taken immediately after the treatment, the results would not directly contradict the results of our study. Käferböck et al. (2020) investigated the effect of PEF on *Arthrospira maxima*, a close relative of *A. platensis* with similar cell morphology and pigment composition (Vonshak, 1997). With electric field strengths between 15 and 25 kV cm^{-1}, the treatment conditions are comparable to our study. The reported data show a field strength dependency of the time-dependent PC yield but no lag time, which might be due to the fact that the first data point was taken after 30 min. Furthermore, they investigated the effect of PEFs by scanning electron microscopy. The images published revealed a lesion of the trichome and the release of unidentified substances, but the overall structure seems to stay intact. This is somewhat contradictory to the results of this study and the results of Jaeschke et al., in which particle decay triggered by the PEF treatment was observed. However, Carullo et al. (2021) and Käferböck et al. did not specify the time after the treatment at which the images of the trichomes were taken.

Accuracy of the Image Processing Algorithm

As our results rely on the accuracy of the developed image processing algorithm, a more detailed evaluation seems appropriate. An example of the processing of the light microscopy images is shown for one image in **Figure 7**. The Figure shows that trichomes and fragments of different sizes are well-detected by the algorithm (cf. subframe A). In addition, larger agglomerates of trichomes are accurately sorted out. However, **Figure 7** also shows that the code is vulnerable to certain sources of error. For example, parallel trichomes or fragments that are close together can be detected as one cell (cf. subframe B). In addition, impurities on the slide can potentially lead to false detections (cf. subframe C).

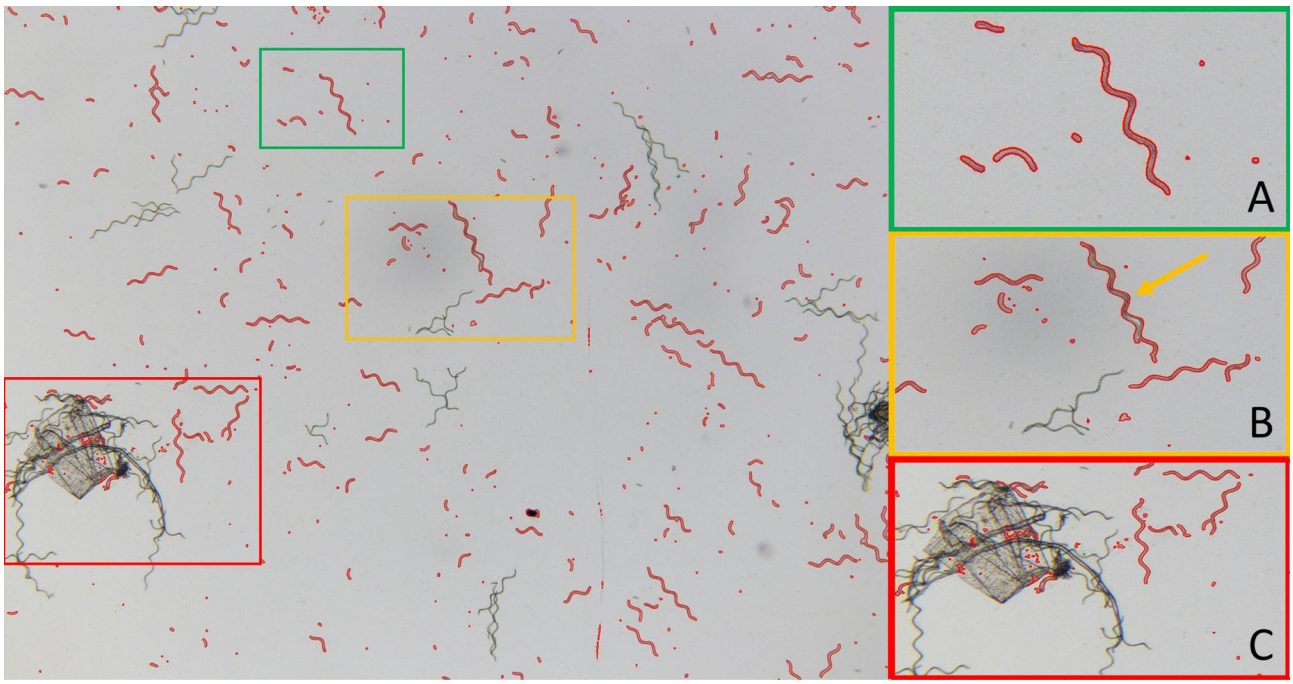

FIGURE 7 | Example image for particle size detection (10 kV cm^{-1}, 60 min). Subframe **(A)** example of successful detection of *A. platensis* trichomes and fragments of different size classes. Subframe **(B)** example of false detection of two *A. platensis* trichomes that are nested together and detected as one particle (cf. yellow arrow). Subframe **(C)** example of false detections due to contamination.

To evaluate the accuracy of the image processing algorithm in a quantitative way, the sensitivity S and false positive rate F were determined according to Equations 3, 4, as described in Section Measurement of Cell Size Distribution. The values are listed in **Table 3**. The sensitivity was $\geq$0.91 for all classes in which particles were detected. This means that at least 91% of objects that are *Arthrospira* cells are also detected by the algorithm. This value shows that particle detection is basically reliable. The false positive rate F for the classes takes on ascending values between 0.13 (1,800–5,000 pixels) and 0.624 (10–100 pixels). This means that large trichomes that have not yet disintegrated can be better distinguished from impurities and agglomerates than from small cell fragments. On the other hand, very small fragments cannot be resolved anymore because of constraints given by the image resolution. Thus, the average particle size, as shown in **Figure 6**, might be overestimated for smaller particles. Nevertheless, the method is suitable for showing the time-dependent decay of trichomes. However, for accurate measurement of small particle sizes, the method must be further refined. One possibility, for example, would be the combination with fluorescence microscopy. This technology allows for better differentiation between smaller cell debris and dirt particles based on the intrinsic fluorescence of pigments such as chlorophyll or PC (Sandmann et al., 2017, 2018). Such a microscopy-based approach for the investigation of single cells would provide information not only on cell size but also on the pigmentation of cells and, thus, their vitality.

Relationship Between Particle Decay and Phycocyanin Release

The previous discussion suggests that the decay of trichomes might be an important mechanism for the release of metabolites such as PC. However, it cannot be clarified without a doubt whether PEFs only trigger a disintegration of trichomes into individual cells or whether the cells also dissolve completely. In the first case, an increase in phycocyanin should start simultaneously with a decline in average cell size, whereas a time shift between the decrease in cell size and the release of the pigment should be measurable in the second case. To test this hypothesis, an experiment was performed directly examining the relationship between the extraction kinetics for phycocyanin and trichome decay. For this purpose, different samples were treated at the same field strength (20 kV cm^{-1}) and temperature (40°C) but different specific energy inputs (25 kJ kg^{-1}, 32 pulses, and 10 kJ kg^{-1}, eight pulses). The higher specific energy input resulted in complete permeabilization (Z_D =1) in the first experimental series, while the lower one resulted in permeabilization of $Z_D = 0.5$ (cf. **Figure 4**).

The results for PC extraction and trichome decay for the two PEF-treated and the untreated samples as well as a sonicated control sample are shown in **Figure 8**. For the untreated sample and PEF-treated sample A (10 kJ kg^{-1}), no change in average particle size was observed. The measured values fluctuate around a mean of 110 µm over the entire extraction time of 240 min. Correspondingly, no increase in PC concentration was measured in the supernatant for both samples. The average particle size of

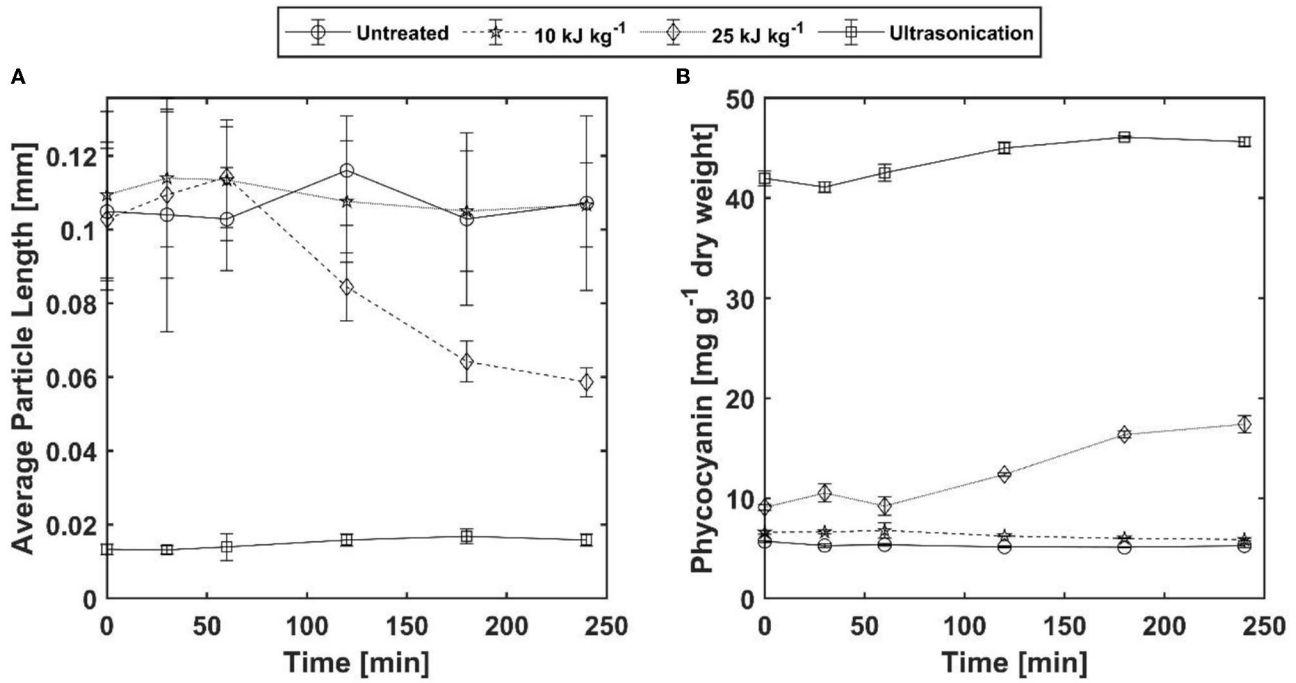

FIGURE 8 | Comparison between decay of *A. platensis* trichomes and phycocyanin extraction yield for one untreated (Sample 0), two PEF-treated [samples **(A,B)**], and one ultrasound-treated sample (sample US). The PEF treatments [**(A)** 10 and **(B)** 25 kJ kg^{-1}] were both carried out at 40°C and 20 kV cm^{-1} with different pulse counts (8 and 32 pulses respectively). Left: Changes in average particle size over a period of 240 min. The error bars indicate the variation of particle length for all detected particles. Right: Phycocyanin extraction over the same time. The error bars indicate the standard deviation from two independent measurements.

the sonicated sample is determined as 13 µm at the beginning of the extraction time. This value does not change during the extraction time. Nevertheless, a slight increase in PC yield from 41 to 45 mg g^{-1} dry weight was measured. One possible explanation for this is that the image processing algorithm used was no longer able to detect particles. While small particles were still visible under the microscope after 0 and 30 min, these had completely dissolved after 60 min. As a result, proportionally more dirt particles were detected, which can falsify the result. The PEF-treated sample B (25 kJ kg^{-1}) also showed no change in average particle size over the first 60 min of the extraction time. After 60 to 120 min, however, the particles began to decay. This is equally reflected in the extraction curve for PC. The average particle size seems to converge to a minimum value of about 60 µm, which also results in a plateau in the extraction yield.

The extract purity, calculated according to Equation 6varied between 0.5 for ultrasonication and 0.73 for PEF sample B. This illustrates the advantage of PEFs compared to other methods such as ultrasound, since a purer extract is obtained despite particle disintegration. The purity of the extract from the sonicated samples is also overestimated, since only cyclic amino acids are measured at the wavelength of 280 nm. The sample showed a dark green color, which indicates that nonpolar substances such as chlorophyll were extracted as well. A possible explanation is that microemulsions are formed because the ultrasonic treatment enhances the solubility of nonpolar substances in polar solvents (Jalali-Jivan et al., 2019; Martínez et al., 2020).

The results shown in **Figure 8** deviate to a certain extent from the results presented above. Since the parameter space for this experiment was chosen based on the first experimental series, it was expected that for PEF sample B, complete permeabilization of the membrane (Z_D =1) and complete disintegration of the trichomes should be observed (cf. **Figures 3**, **5**). However, this was not the case, as the disintegration started later and was also not complete. A possible explanation for this deviation might be that the culture was harvested in the stationary phase on the day of the experiment. This presumption is substantiated by the fact that we observed that the filterability of the culture was worse, and the filter cake showed a slimy consistency. The cells also appeared larger under the microscope. Furthermore, the maximum measured PC yield was relatively low at 45 mg g^{-1} dry weight. According to the literature, the cell can contain up to 20% (200 mg g^{-1} dry weight) of PC (Christaki et al., 2015). Since this is degraded under nitrogen deficiency and serves as a nitrogen source for the cells (Boussiba and Richmond, 1980), nitrogen deficiency is very likely the reason for the variation between the experiments. It has been reported in the literature that *A. platensis* forms more exopolysaccharides (EPSs) under poor conditions such as nitrogen deficiency or high light radiation (Li et al., 2001; Jung et al., 2022). EPSs form a layer around trichomes and protect them from environmental stress such as dehydration.

This layer might protect the cells and prevent them from breaking apart (Pereira et al., 2009), which may have caused the observed differences in our first experimental series.

Nevertheless, the results in **Figure 8** show for the first time that the decay of trichomes is directly accompanied by the release of PC. Since the release of PC starts simultaneously with the disintegration of trichomes, it can be assumed that all the experiments shown in **Figure 5** should also lead to a complete release of PC. Further evaluation of this hypothesis will be the subject of our future research.

CONCLUSION

In this study, for the first time, the permeabilization of *Arthrospira platensis* by PEFs was directly measured by fluorescence spectroscopy and using propidium iodide as the dye. This novel method enables a deeper understanding of the interaction of electric field strength, treatment temperature, and treatment time and their compensating effects for the permeabilization of the cell membrane. It has been demonstrated that treatment with an electric field strength of 15 kV cm^{-1} or higher is sufficient to permeabilize 100% of the trichomes for PI. Nevertheless, significant differences regarding the required treatment time for full permeabilization were observed depending on the treatment conditions, e.g., temperature and electric field strength. Furthermore, the quantitative digital image analysis showed that cells that were completely permeabilized for PI also completely disintegrated over a period of 180 min. This disintegration seems responsible for the release of the water-soluble pigment PC. Thus, this study is the first to demonstrate the relationship between permeabilization and the kinetics of particle decay and PC extraction.

Although our data demonstrate the time-dependent decay of trichomes after PEF treatment, further questions need to be clarified. As such, the reason for the decay can only be presumed. One possible explanation is that cellular enzymes decompose the trichomes after cell death caused by PEFs. This has already been described for other phototrophic microorganisms in the literature (Martínez et al., 2019; Scherer et al., 2019; Canelli et al., 2022). Besides the temperature dependencies of mass transfer and solubility, such as a causal mechanism, would also provide another explanation for the strong dependence of extraction kinetics for different cell metabolites on environmental conditions (Akaberi et al., 2020). Therefore, this aspect should be further investigated in future research. Furthermore, our results bring up interesting new research questions regarding the relationship between growth phase at harvest and sensitivity of trichomes to treatment with PEF. The knowledge gained through this study simplifies the design of downstream processes and thus contributes to the successful introduction of *A. platensis* on the market as a source of proteins for human nutrition.

DATA AVAILABILITY STATEMENT

The raw data supporting the conclusions of this article will be made available by the authors, without undue reservation.

AUTHOR CONTRIBUTIONS

JK and CM conceptualized the study and drafted the manuscript. JK supervised the experimental work and analyzed the experimental data. JK, JN, NF, and YY conducted the experiments. NF developed the used PI staining protocol in the context of her final thesis. JN adapted the staining protocol to the strain used in this study. CR and CL critically revised the manuscript and improved the study with important intellectual content. CM and CR took responsibility for the integrity of the study. All authors read and approved the submitted manuscript.

FUNDING

This study was funded by the German Federal Ministry of Food and Agriculture as part of the project Antiviral Substances and Pigments (Antivirale Substanzen und Pigmente; Grant No: 2219NR287). The authors acknowledge the support.

ACKNOWLEDGMENTS

The authors thank Irene Hemmerich and Sigrid Drecker for supporting the experiments through practical assistance and advice on methodology.

SUPPLEMENTARY MATERIAL

The Supplementary Material for this article can be found online at: https://www.frontiersin.org/articles/10.3389/fsufs.2022.934552/full#supplementary-material

REFERENCES

Abalde, J., Betancourt, L., Torres, E., Cid, A., and Barwell, C. (1998). Purification and characterization of phycocyanin from the marine cyanobacterium *Synechococcus* sp. IO9201. *Plant Sci.* 136, 109–120. doi: 10.1016/S0168-9452(98)00113-7

Abel, G. J., Barakat, B., Kc, S., and Lutz, W. (2016). Meeting the Sustainable Development Goals leads to lower world population growth. *Proc. Natl. Acad. Sci. U. S. A.* 113, 14294–14299. doi: 10.1073/pnas.1611386113

Akaberi, S., Krust, D., Müller, G., Frey, W., and Gusbeth, C. (2020). Impact of incubation conditions on protein and C-Phycocyanin recovery from *Arthrospira platensis* post- pulsed electric field treatment. *Bioresour. Technol.* 306:123099. doi: 10.1016/j.biortech.2020.123099

Aouir, A., Amiali, M., Kirilova-Gachovska, T., Benchabane, A., and Bitam, A. (2015). "The effect of pulsed electric field (PEF) and ultrasoud (US) technologies on the extraction of phycopiliproteins from Arthrospira platensis," in *2015 IEEE Canada International Humanitarian Technology Conference (IHTC), Ottawa, Canada, May 31 to June 4 2015*, 1–4.

Becker, E. W. (2007). Micro-algae as a source of protein. *Biotechnol. Adv.* 25, 207–210. doi: 10.1016/j.biotechadv.2006.11.002

Becker, E. W. (2013). "Microalgae in human and animal nutrition," in *Handbook of Microalgal Culture: Applied Phycology and Biotechnology*, eds A. Richmond, and Q. Hu (Hoboken, NJ: Wiley Blackwell), 312–351. doi: 10.1002/9780470995280.ch18

Benelhadj, S., Gharsallaoui, A., Degraeve, P., Attia, H., and Ghorbel, D. (2016). Effect of pH on the functional properties of *Arthrospira*

(Spirulina) platensis protein isolate. *Food Chem.* 194, 1056–1063. doi: 10.1016/j.foodchem.2015.08.133

Bennett, A., and Bogorad, L. (1973). Complementary chromatic adaptation in a filamentous blue-green alga. *J. Cell Biol.* 58, 419–435. doi: 10.1083/jcb.58.2.419

Bertsch, P., Böcker, L., Mathys, A., and Fischer, P. (2021). Proteins from microalgae for the stabilization of fluid interfaces, emulsions, and foams. *Trends Food Sci. Technol.* 108, 326–342. doi: 10.1016/j.tifs.2020.12.014

Böcker, L., Bertsch, P., Wenner, D., Teixeira, S., Bergfreund, J., Eder, S., et al. (2021). Effect of Arthrospira platensis microalgae protein purification on emulsification mechanism and efficiency. *J. Colloid Interface Sci* 584, 344–353. doi: 10.1016/j.jcis.2020.09.067

Böcker, L., Hostettler, T., Diener, M., Eder, S., Demuth, T., Adamcik, J., et al. (2020). Time-temperature-resolved functional and structural changes of phycocyanin extracted from *Arthrospira platensis/Spirulina*. *Food Chem.* 316:126374. doi: 10.1016/j.foodchem.2020.126374

Boer, K., de, Moheimani, N. R., Borowitzka, M. A., and Bahri, P. A. (2012). Extraction and conversion pathways for microalgae to biodiesel: a review focused on energy consumption. *J. Appl. Phycol.* 24, 1681–1698. doi: 10.1007/s10811-012-9835-z

Boussiba, S., and Richmond, A. E. (1980). C-phycocyanin as a storage protein in the blue-green alga *Spirulina platensis*. *Arch. Microbiol.* 125, 143–147. doi: 10.1007/BF00403211

Buchmann, L., and Mathys, A. (2019). Perspective on pulsed electric field treatment in the bio-based industry. *Front. Bioeng. Biotechnol.* 7:265. doi: 10.3389/fbioe.2019.00265

Canelli, G., Kuster, I., Jaquenod, L., Buchmann, L., Murciano Martínez, P., Rohfritsch, Z., et al. (2022). Pulsed electric field treatment enhances lipid bioaccessibility while preserving oxidative stability in *Chlorella vulgaris*. *Innov. Food Sci. Emerg. Technol.* 75:102897. doi: 10.1016/j.ifset.2021.102897

Caporgno, M. P., and Mathys, A. (2018). Trends in microalgae incorporation into innovative food products with potential health benefits. *Front. Nutr.* 5:58. doi: 10.3389/fnut.2018.00058

Carullo, D., Abera, B. D., Casazza, A. A., Dons,ì, F., Perego, P., Ferrari, G., et al. (2018). Effect of pulsed electric fields and high pressure homogenization on the aqueous extraction of intracellular compounds from the microalgae *Chlorella vulgaris*. *Algal Res.* 31, 60–69. doi: 10.1016/j.algal.2018.01.017

Carullo, D., Abera, B. D., Scognamiglio, M., Dons,ì, F., Ferrari, G., and Pataro, G. (2022). Application of pulsed electric fields and high-pressure homogenization in biorefinery cascade of *C. vulgaris* Microalgae. *Foods* 11:30471. doi: 10.3390/foods11030471

Carullo, D., Dons,ì, F., Ferrari, G., and Pataro, G. (2021). Extraction improvement of water-soluble compounds from *Arthrospira platensis* through the combination of high-shear homogenization and pulsed electric fields. *Algal Res.* 57:102341. doi: 10.1016/j.algal.2021.102341

Carullo, D., Pataro, G., Dons,ì, F., and Ferrari, G. (2020). Pulsed electric fields-assisted extraction of valuable compounds from *Arthrospira platensis*: effect of pulse polarity and mild heating. *Front. Bioeng. Biotechnol.* 8:551272. doi: 10.3389/fbioe.2020.551272

Carvalho, J. C., de Magalhães, A. I., Melo Pereira, G. V., de Medeiros, A. B. P., Sydney, E. B., Rodrigues, C., et al. (2020). Microalgal biomass pretreatment for integrated processing into biofuels, food, and feed. *Bioresour. Technol.* 300:122719. doi: 10.1016/j.biortech.2019.122719

Chew, K. W., Yap, J. Y., Show, P. L., Suan, N. H., Juan, J. C., Ling, T. C., et al. (2017). Microalgae biorefinery: high value products perspectives. *Bioresour. Technol.* 229, 53–62. doi: 10.1016/j.biortech.2017.01.006

Christaki, E., Bonos, E., and Florou-Paneri, P. (2015). "Innovative microalgae pigments as functional ingredients in nutrition," in *Handbook of Marine Microalgae*, ed S-K. Kim (Amsterdam: Elsevier), 233–243. doi: 10.1016/B978-0-12-800776-1.00014-5

Goettel, M., Eing, C., Gusbeth, C., Straessner, R., and Frey, W. (2013). Pulsed electric field assisted extraction of intracellular valuables from microalgae. *Algal Res.* 2, 401–408. doi: 10.1016/j.algal.2013.07.004

Grossmann, L., Hinrichs, J., and Weiss, J. (2020). Cultivation and downstream processing of microalgae and cyanobacteria to generate protein-based technofunctional food ingredients. *Crit. Rev. Food Sci. Nutr.* 60, 2961–2989. doi: 10.1080/10408398.2019.1672137

Heinz, V., Alvarez, I., Angersbach, A., and Knorr, D. (2001). Preservation of liquid foods by high intensity pulsed electric fields—basic concepts for process design. *Trends Food Sci. Technol.* 12, 103–111. doi: 10.1016/S0924-2244(01)00064-4

Jaeschke, D. P., Mercali, G. D., Marczak, L. D. F., Müller, G., Frey, W., and Gusbeth, C. (2019). Extraction of valuable compounds from *Arthrospira platensis* using pulsed electric field treatment. *Bioresour. Technol.* 283, 207–212. doi: 10.1016/j.biortech.2019.03.035

Jalali-Jivan, M., Abbasi, S., and Scanlon, M. G. (2019). Microemulsion as nanoreactor for lutein extraction: optimization for ultrasound pretreatment. *J. Food Biochem.* 43:e12929. doi: 10.1111/jfbc.12929

Jung, S.-H., Zell, Niklas: Boßle, Fabian, T.eipel, U., Rauh, C., McHardy, C., and Lindenberger, C. (2022). Influence of process operation on the production of exopolysaccharides in *Arthrospira platensis* and *Chlamydomonas asymmetrica*. *Front. Sustain. Food Proces.* 2022:883069. doi: 10.3389/fsufs.2022.883069

Käferböck, A., Smetana, S., Vos, R., de, Schwarz, C., Toepfl, S., and Parniakov, O. (2020). Sustainable extraction of valuable components from Spirulina assisted by pulsed electric fields technology. *Algal Res.* 48:101914. doi: 10.1016/j.algal.2020.101914

Kim, Z.-H., Park, H., Hong, S.-J., Lim, S.-M., and Lee, C.-G. (2016). Development of a floating photobioreactor with internal partitions for efficient utilization of ocean wave into improved mass transfer and algal culture mixing. *Bioprocess Biosyst. Eng.* 39, 713–723. doi: 10.1007/s00449-016-1552-6

Knappert, J., McHardy, C., and Rauh, C. (2020). Kinetic modeling and numerical simulation as tools to scale microalgae cell membrane permeabilization by means of pulsed electric fields (PEF) from lab to pilot plants. *Front. Bioeng. Biotechnol.* 8:209. doi: 10.3389/fbioe.2020.00209

Lam, G. P. 't., Postma, P. R., Fernandes, D. A., Timmermans, R. A. H., Vermuë, M. H., Barbosa, M. J., et al. (2017a). Pulsed Electric Field for protein release of the microalgae *Chlorella vulgaris* and Neochloris oleoabundans. *Algal Res.* 24, 181–187. doi: 10.1016/j.algal.2017.03.024

Lam, G. P. 't., van der Kolk, J. A., Chordia, A., Vermuë, M. H., Olivieri, G., Eppink, M. H. M., et al. (2017b). Mild and selective protein release of cell wall deficient microalgae with pulsed electric field. *ACS Sustain. Chem. Eng.* 5, 6046–6053. doi: 10.1021/acssuschemeng.7b00892

Lebovka, N. I., Bazhal, M. I., and Vorobiev, E. (2002). Estimation of characteristic damage time of food materials in pulsed-electric fields. *J. Food Eng.* 54, 337–346. doi: 10.1016/S0260-8774(01)00220-5

Leonhardt, L., Käferböck, A., Smetana, S., Vos, R., de Toepfl, S., and Parniakov, O. (2020). Bio-refinery of *Chlorella sorokiniana* with pulsed electric field pre-treatment. *Bioresour. Technol.* 301:122743. doi: 10.1016/j.biortech.2020.122743

Li, P., Harding, S. E., and Liu, Z. (2001). Cyanobacterial exopolysaccharides: their nature and potential biotechnological applications. *Biotechnol. Genet. Eng. Rev.* 18, 375–404. doi: 10.1080/02648725.2001.10648020

Luengo, E., Condón-Abanto, S., Álvarez, I., and Raso, J. (2014). Effect of pulsed electric field treatments on permeabilization and extraction of pigments from *Chlorella vulgaris*. *J. Membr. Biol.* 247, 1269–1277. doi: 10.1007/s00232-014-9688-2

Martelli, G., Folli, C., Visai, L., Daglia, M., and Ferrari, D. (2014). Thermal stability improvement of blue colorant C-Phycocyanin from *Spirulina platensis* for food industry applications. *Process Biochem.* 49, 154–159. doi: 10.1016/j.procbio.2013.10.008

Martínez, J. M., Delso, C., Aguilar, D. E., Álvarez, I., and Raso, J. (2020). Organic-solvent-free extraction of carotenoids from yeast *Rhodotorula glutinis* by application of ultrasound under pressure. *Ultrason Sonochem.* 61:104833. doi: 10.1016/j.ultsonch.2019.104833

Martínez, J. M., Gojkovic, Z., Ferro, L., Maza, M., Álvarez, I., Raso, J., et al. (2019). Use of pulsed electric field permeabilization to extract astaxanthin from the Nordic microalga *Haematococcus pluvialis*. *Bioresour. Technol.* 289:121694. doi: 10.1016/j.biortech.2019.121694

Martínez, J. M., Luengo, E., Saldaña, G., Álvarez, I., and Raso, J. (2017). C-phycocyanin extraction assisted by pulsed electric field from *Artrosphira platensis*. *Food Res. Int.* 99, 1042–1047. doi: 10.1016/j.foodres.2016.09.029

McHardy, C., Djike Kammegne, T., and Jänich, I. (2021). Energy-efficient ultrasound-assisted extraction of food proteins from the microalga *C. vulgaris* at elevated static pressure. *Innov. Food Sci. Emerg. Technol.* 73:102797. doi: 10.1016/j.ifset.2021.102797

Nijdam, D., Rood, T., and Westhoek, H. (2012). The price of protein: review of land use and carbon footprints from life cycle assessments

of animal food products and their substitutes. *Food Policy* 37, 760–770. doi: 10.1016/j.foodpol.2012.08.002

Oliveira, M. A. C. L., de, Monteiro, M. P. C., Robbs, P. G., and Leite, S. G. F. (1999). Growth and chemical composition of *Spirulina maxima* and *Spirulina platensis* biomass at different temperatures. *Aquacult. Int.* 7, 261–275. doi: 10.1023/A:1009233230706

Papachristou, I., Akaberi, S., Silve, A., Navarro-López, E., Wüstner, R., Leber, K., et al. (2021). Analysis of the lipid extraction performance in a cascade process for *Scenedesmus almeriensis* biorefinery. *Biotechnol. Biofuels* 14:20. doi: 10.1186/s13068-020-01870-1

Pataro, G., Goettel, M., Straessner, R., Gusbeth, C., Ferrari, G., and Frey, W. (2017). Effect of pef treatment on extraction of valuable compounds from microalgae *C. vulgaris*. *Chem. Eng. Trans.* 57, 67–72. doi: 10.3303/CET1757012

Pataro, G., Senatore, B., Dons,ì, G., and Ferrari, G. (2011). Effect of electric and flow parameters on PEF treatment efficiency. *J. Food Eng.* 105, 79–88. doi: 10.1016/j.jfoodeng.2011.02.007

Pereira, S., Zille, A., Micheletti, E., Moradas-Ferreira, P., Philippis, R., de, and Tamagnini, P. (2009). Complexity of cyanobacterial exopolysaccharides: composition, structures, inducing factors and putative genes involved in their biosynthesis and assembly. *FEMS Microbiol. Rev.* 33, 917–941. doi: 10.1111/j.1574-6976.2009.00183.x

Pleonsil, P., Soogarun, S., and Suwanwong, Y. (2013). Anti-oxidant activity of holo- and apo-c-phycocyanin and their protective effects on human erythrocytes. *Int. J. Biol. Macromol.* 60, 393–398. doi: 10.1016/j.ijbiomac.2013.06.016

Poore, J., and Nemecek, T. (2018). Reducing food's environmental impacts through producers and consumers. *Science* 360, 987–992. doi: 10.1126/science.aaq0216

Postma, P. R., Pataro, G., Capitoli, M., Barbosa, M. J., Wijffels, R. H., Eppink, M. H. M., et al. (2016). Selective extraction of intracellular components from the microalga *Chlorella vulgaris* by combined pulsed electric field-temperature treatment. *Bioresour. Technol.* 203, 80–88. doi: 10.1016/j.biortech.2015.12.012

Postma, P. R., Suarez-Garcia, E., Safi, C., Yonathan, K., Olivieri, G., Barbosa, M. J., et al. (2017). Energy efficient bead milling of microalgae: effect of bead size on disintegration and release of proteins and carbohydrates. *Bioresour. Technol.* 224, 670–679. doi: 10.1016/j.biortech.2016.11.071

Ramírez-Rodrigues, M. M., Estrada-Beristain, C., Metri-Ojeda, J., Pérez-Alva, A., and Baigts-Allende, D. K. (2021). *Spirulina platensis* protein as sustainable ingredient for nutritional food products development. *Sustainability* 13:6849. doi: 10.3390/su13126849

Ruiz, J., Olivieri, G., Vree, J., de, Bosma, R., Willems, P., Reith, J. H., et al. (2016). Towards industrial products from microalgae. *Energy Environ. Sci.* 9, 3036–3043. doi: 10.1039/C6EE01493C

Sandmann, M., Lippold, M., Saalfrank, F., Odika, C. P., and Rohn, S. (2017). Multidimensional single-cell analysis based on fluorescence microscopy and automated image analysis. *Anal. Bioanal. Chem.* 409, 4009–4019. doi: 10.1007/s00216-017-0344-4

Sandmann, M., Schafberg, M., Lippold, M., and Rohn, S. (2018). Analysis of population structures of the microalga *Acutodesmus obliquus* during lipid production using multi-dimensional single-cell analysis. *Sci. Rep.* 8:6242. doi: 10.1038/s41598-018-24638-y

Saulis, G. (2010). Electroporation of cell membranes: the fundamental effects of pulsed electric fields in food processing. *Food Eng. Rev.* 2, 52–73. doi: 10.1007/s12393-010-9023-3

Scherer, D., Krust, D., Frey, W., Mueller, G., Nick, P., and Gusbeth, C. (2019). Pulsed electric field (PEF)-assisted protein recovery from *Chlorella vulgaris* is mediated by an enzymatic process after cell death. *Algal Res.* 41:101536. doi: 10.1016/j.algal.2019.101536

Shanab, S. M. M., Mostafa, S. S. M., Shalaby, E. A., and Mahmoud, G. I. (2012). Aqueous extracts of microalgae exhibit antioxidant and anticancer activities. *Asian Pacific J. Trop. Biomed.* 2, 608–615. doi: 10.1016/S2221-1691(12)60106-3

Sigurdson, G. T., Tang, P., and Giusti, M. M. (2017). Natural colorants: food colorants from natural sources. *Annu. Rev. Food Sci. Technol.* 8, 261–280. doi: 10.1146/annurev-food-030216-025923

Stadnichuk, I. N., Krasilnikov, P. M., and Zlenko, D. V. (2015). Cyanobacterial phycobilisomes and phycobiliproteins. *Microbiology* 84, 101–111. doi: 10.1134/S0026261715020150

Tomaselli, L. (1997). "Morphology, ultrastructure and taxonomy of *Arthrospira (Spirulina) maxima* and *Arthrospira (Spirulina) platensis*," in *Spirulina platensis Arthrospira: Physiology, Cell-Biology and Biotechnology*, ed A. Vonshak (Hoboken, NJ: Taylor and Francis), 1–15.

van Krimpen, M. M., Bikker, P., van der Meer, I. M., van der Peet-Schwering, C. M. C., and Vereijken, J. M. (2013). *Cultivation, Processing and nutritional Aspects for Pigs and Poultry of European Protein Sources as Alternatives for Imported Soybean Products*. Wageningen: Wageningen Livestock Research.

Vonshak, A. (1997). *Spirulina platensis Arthrospira: Physiology, Cell-Biology and Biotechnology*. Hoboken, NJ: Taylor and Francis. doi: 10.1201/9781482272970

Zheng, J., Inoguchi, T., Sasaki, S., Maeda, Y., McCarty, M. F., Fujii, M., et al. (2013). Phycocyanin and phycocyanobilin from *Spirulina platensis* protect against diabetic nephropathy by inhibiting oxidative stress. *Am. J. Physiol. Regul. Integr. Comp. Physiol.* 304, R110–R120. doi: 10.1152/ajpregu.00648.2011

Conflict of Interest: The authors declare that the research was conducted in the absence of any commercial or financial relationships that could be construed as a potential conflict of interest.

Publisher's Note: All claims expressed in this article are solely those of the authors and do not necessarily represent those of their affiliated organizations, or those of the publisher, the editors and the reviewers. Any product that may be evaluated in this article, or claim that may be made by its manufacturer, is not guaranteed or endorsed by the publisher.